




Direct-Deposited Graphene Oxide on Dental Implants for Antimicrobial Activities and Osteogenesis

WooHyung Jang ¹

Hee-Seon Kim¹

Khurshed Alam ²

Min-Kyung Ji³

Hoon-Sung Cho ²

Hyun-Pil Lim¹

¹Department of Prosthodontics, School of Dentistry, Chonnam National University, Gwangju, Korea; ²Department of Materials Science and Engineering, Chonnam National University, Gwangju, 61186, Korea; ³Optoelectronics Convergence Research Center, Chonnam National University, Gwangju, 61186, Korea

Objective: To determine the effects of graphene oxide (GO) deposition (on a zirconia surface) on bacterial adhesion and osteoblast activation.

Methods: An atmospheric pressure plasma generator (PGS-300) was used to coat Ar/CH₄ mixed gas onto zirconia specimens (15-mm diameter × 2.5-mm thick disks) at a rate of 10 L/min and 240 V. Zirconia specimens were divided into two groups: uncoated (control; Zr) group and GO-coated (Zr-GO) group. Surface characteristics and element structures of each specimen were evaluated by field emission scanning electron microscope (FE-SEM), X-ray photoelectron spectroscopy (XPS), Raman spectroscopy, and contact angle. Additionally, crystal violet staining was performed to assess the adhesion of *Streptococcus mutans*. WST-8 and ALP (Alkaline phosphatase) assays were conducted to evaluate MC3T3-E1 osteoblast adhesion, proliferation, and differentiation. Statistical analysis was calculated by the Mann-Whitney *U*-test.

Results: FE-SEM and Raman spectroscopy demonstrated effective GO deposition on the zirconia surface in Zr-GO. The attachment and biofilm formation of *S. mutans* was significantly reduced in Zr-GO compared with that of Zr ($P < 0.05$). While no significant differences in cell attachment of MC3T3-E1 were observed, both proliferation and differentiation were increased in Zr-GO as compared with that of Zr ($P < 0.05$).

Significance: GO-coated zirconia inhibited the attachment of *S. mutans* and stimulated proliferation and differentiation of osteoblasts. Therefore, GO-coated zirconia can prevent peri-implantitis by inhibiting bacterial adhesion. Moreover, its osteogenic ability can increase bone adhesion and success rate of implants.

Keywords: graphene oxide, GO, zirconia implant, biofilm formation, osteoblast, non-thermal atmospheric pressure plasma

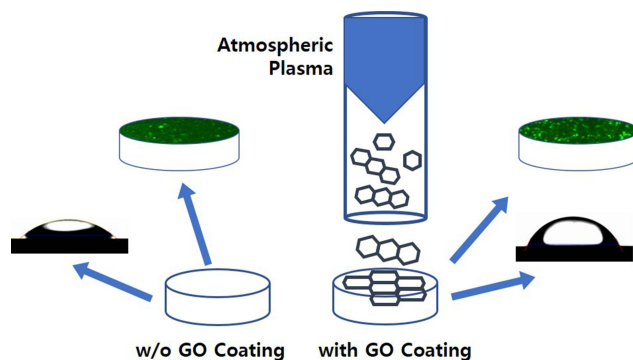
Correspondence: Hyun-Pil Lim
Department of Prosthodontics, School of Dentistry, Chonnam National University, Gwangju, 61186, Korea
Tel +82-10-2645-7528
Fax +82-62-530-5577
Email mcnihil@jnu.ac.kr

Hoon-Sung Cho
Department of Materials Science and Engineering, Chonnam National University, Gwangju, 61186, Korea
Tel/Fax +82-62-530-1717
Email cho.hoonsung@jnu.ac.kr

Introduction

Peri-implantitis is the most significant cause of early or late implant failures.¹ It occurs when bacteria coagulate irreversibly on the teeth or implants and leads to the formation of a bacterial biofilm on the surface, which can lead to bone loss.²⁻⁴ To treat peri-implantitis, mechanical methods which remove the biofilm using carbon fiber curettes and chemical methods which kill the bacteria via disinfection treatment and antibiotics⁵⁻⁷ are used together for effective results. Recently, to prevent peri-implantitis, many attempts have been made to treat the surface of implants with antibacterial materials.⁸ Graphene, a honeycomb-lattice monolayer comprising aromatic ring carbon atoms, is a potential biomaterial owing to its unique physical and

Graphical Abstract



chemical properties.^{9–11} In contrast, unlike graphene, graphene oxide (GO) has hydrophilic tendency because of its functional groups (ie, carboxyl, hydroxyl, and epoxy groups); an antibiotic effect; and it promotes bone production through osteoblast activation.^{12–17} Existing methods of GO fabrication include chemical or physical exfoliation from bulk graphite,^{18,19} chemical vapor deposition using a metal catalyst,²⁰ and Hummer's method.^{21,22} However, these methods have some disadvantages including high pollution, low efficiency, potential residual solution byproducts used in GO production, and the generation of harmful inflammable gases such as NO₂, N₂O₄, and ClO₂.^{23–25}

When living tissues are treated with plasma (a charged gas because of ionized energy), their wettability and mechanical and biological properties can be modified.²⁶ Plasma treatment improves biocompatibility, cell adhesion, and increases bacterial resistance.^{27–30} In this study, we developed a new method combining plasma treatment and graphene synthesis. Rho et al reported the deposition of an argon plasma-based GO on a titanium surface, improving biocompatibility and promoting differentiation of fibroblasts (NCTC clone 929) and MC3T3-E1 cells.³¹ This simple and cost-effective method did not require any additives or produced any by-products. Zirconia, one of the primary dental materials, has low toxicity and corrosivity and high antibiotic activity and biocompatibility.^{32,33} Owing to these features, zirconia implants are currently being studied extensively. The increase in clinical applications of zirconia implants is because of its higher success rate³⁴ and comparable fracture strength to that of titanium, which has been widely used in the past.³⁵

However, to the best of our knowledge, the combined effects of GO and zirconia have not yet been reported. Therefore, this study evaluated the effects of a biocompatible plasma-based GO-coated Zr surface on biofilm formation and osteoblast activation.

Materials and Methods

Experimental Materials

Samples

Zirconia (Zirmon, Kuwotech, Gwangju, Korea) was produced into disk-shaped specimens (diameter: 15 mm, thickness: 2.5 mm). The surface of each specimen was prepared using #800 SiC (silicon carbide) paper to obtain an even surface. All specimens were cleaned with acetone, alcohol, and distilled water for 20 min using an ultrasonic cleaner. Thereafter, the specimens were dried at room temperature (20–25 °C) and sterilized using an autoclave (HS-3460SD, Hanshin Medical Co, Korea). Two groups of zirconia specimens were prepared: pure zirconia specimens which were not coated with GO (Group Zr) and zirconia specimens which were coated with GO for 1 min (Group Zr-GO).

GO-Coated Zirconia

Zirconia specimens were coated with GO using an atmospheric pressure plasma generator (PGS-300, Expantech Co, Korea). Argon gas (4 L/min) and methane gas (3.5 mL/min) were mixed in a quartz tube and coated on the surface at 240 V at the rate of 10 L/min. The distance between the specimen and plasma was maintained at 25 mm, and the plasma was rotated and simultaneously

Table 1 Parameters of the Atmospheric Plasma Generator

Parameter	Value
Average working power (W)	240
Voltage (V)	27
Frequency (MHz)	900
Atmospheric pressure (Torr)	760
Electrode type	Electrodeless
Cooling type	Air-cooled
Plasma density	$10^{15}/\text{cm}^3$

reciprocated from side-to-side to ensure even application of GO on the surface (Table 1, Figure 1).

Assessment of Surface Characteristics

The surface of zirconia was coated with platinum in vacuum for 60 s using a sputter coater (E-1030, Hitachi, Japan) and was observed using a field emission scanning electron microscope (FE-SEM; S-4700, Hitachi, Japan).

The thicknesses, atomic components, and chemical bonds of the specimens were assessed using X-ray photoelectron spectroscopy (XPS; VG Multilab 2000, Thermo Scientific, UK). The peak areas of atomic elements observed in the specimens were normalized and expressed as quantitative proportions.

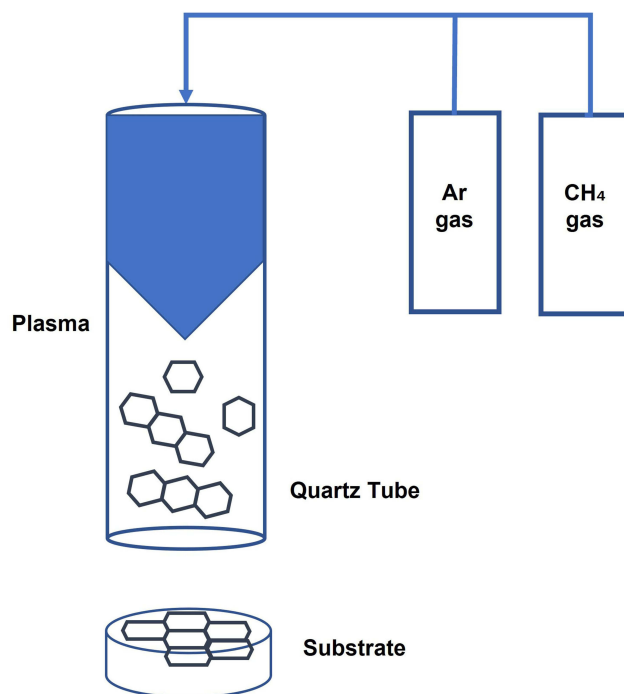


Figure 1 Schematic diagram of GO coating with atmospheric plasma generator.

The shapes, thicknesses, and roughness of specimens were observed using a nanosurface 3D optical profiler (NV-E1000, Nano System, Korea), and for each group three specimens were measured using three different areas.

Raman spectroscopy was performed to assess the status of the GO coating on the zirconia surface at 532.13 nm using a Raman spectrometer (NRS-5100, JASCO, Japan), and the contact angle (Phoenix 300, SEO Inc., Korea) was measured to compare the hydrophilicity of the surfaces. For each group, three specimens were measured and their average contact angles were analyzed (Surfaceware 9 software, SEO Inc, Korea)

Assessment of Bacterial Adhesion

Bacterial Culture

To evaluate biofilm thickness inhibition, *Streptococcus mutans* (KCOM 1504 obtained from the Korean Collection for Oral Microbiology (KCOM, Korea)), a gram-positive bacterium involved in early biofilm formation, was used. *S. mutans* was cultured at 37 °C in a culture chamber (LIB-150M, DAIHAN Labtech Co., Korea) using a BHI medium (Brain Heart Infusion, Becton, Dickinson and Company, Sparks, MD, USA).

Bacterial Inoculation

Every specimen was sterilized in an autoclave (HS-3460SD, Hanshin Medical Co, Korea) for 2 h and disinfected under UV for 24 h. Subsequently, for each group, eight specimens were placed in a 24-well plate (SPL Life Sciences Co., Ltd., Korea), and each specimen was inoculated with *S. mutans* (1.5×10^7 CFU/mL) and cultured for 24 h.

Bacterial Adhesion Assessment

After culturing, the culture medium was removed, and the specimens were cleaned with Phosphate Buffer Saline (PBS) solution twice. Adherent bacteria were dyed with 0.3% crystal violet solution by dispensing 500 μL of the solution to each specimen. After 10 min, the crystal violet solution was removed, and the remaining solution was cleaned three times with PBS solution. Subsequently, the specimens were dried for 15 min, and 500 μL of demineralized solution (80% ethyl alcohol + 20% acetone) was dispensed. The specimens were tightly sealed and stirred for 1 h. After stirring, 200 μL of each specimen was dispensed into a 96-well plate (SPL Life Sciences Co, Ltd, Korea), and their absorbance was measured at 595 nm using ELISA (VersaMax ELISA Microplate Reader, Molecular Device, CA, USA).

Bacteria adhesion was visually assessed using the LIVE/DEAD[®] BacLight[™] Bacterial Viability Kit (SYTO 9[®], Molecular Probes Europe BV, Netherlands). After culturing, the bacteria and the remaining culture medium were cleaned with PBS solution. To each specimen, 200 μL of fluorescence reagent (SYTO 9 dye: propidium iodide: dH_2O = 1.5 μL : 1.5 μL : 1.0 mL) was injected. The well plate was sealed with aluminum foil to block the light and was dyed at room temperature (20–25 $^\circ\text{C}$) for 15 min. Subsequently, the remaining dye solution was cleaned with PBS solution and the adherent bacteria were observed using a confocal laser scanning microscope (Leica TCS SP5 AOBS/tandem, Leica, Germany) and the thickness of the biofilm formed on the specimen was measured through an z-axis depth profiling (Leica LAS AF software, Leica Microsystems, Bensheim, Germany).

Assessment of Osteoblast Viability

Cell Culture

MC3T3-E1 osteoblasts (MC3T3-E1 subclone 4, ATCC CRL2593, USA) were cultured at 37 $^\circ\text{C}$ in a 5% CO_2 incubator (Forma Series II 3111 Water Jacketed CO_2 Incubator, Thermo Fisher Scientific Inc., USA) using an alpha minimum essential medium (α -MEM; Gibco-BRL, Grand Island, USA) containing 10% fetal bovine serum (FBS) and 100 U/mL penicillin.

Cell Adhesion/Proliferation

For each group, eight specimens were prepared and fixed in a 24-well plate. Cultured cells (4×10^4 cells/mL) were dispensed on each specimen and incubated at 37 $^\circ\text{C}$ in a 5% CO_2 incubator. After dispensing the cells, cell adhesion and proliferation were assessed on the 1st and the 5th day, respectively. Before assessment, the surface was cleaned with PBS to remove any remaining culture medium and non-adherent cells. Subsequently, 1 mL of fresh medium and 100 μL of WST-8 reagent (EZ-Cytox, Itsbio, Inc., Korea) were added to each specimen and incubated at 37 $^\circ\text{C}$ in a 5% CO_2 incubator. After 10 min, when color development was observed, 100 μL of each specimen was dispensed into a 96-well plate and their absorbance was measured at 450 nm using an absorbance reader (VersaMax ELISA Microplate Reader, Molecular Devices, USA).

Cell Differentiation

For each group, eight specimens disinfected with UV rays were fixed in a 24-well plate. Cultured cells (4×10^4 cells/mL) were dispensed on each specimen and cultured at 37 $^\circ\text{C}$ in a 5% CO_2 incubator. Cell differentiation was assessed on the 21st day

after culturing. Subsequently, the surface was cleaned with PBS to remove the remaining culture medium and non-adherent cells. Each specimen was treated with 200 μL of ALP assay buffer and cultured at 37 $^\circ\text{C}$ in a 5% CO_2 incubator for 1 h. Subsequently, 80 μL of each specimen was dispensed into a 96-well plate and treated with 50 μL of pNPP solution. The specimens were cultured at 37 $^\circ\text{C}$ in a 5% CO_2 incubator for 1 h, treated with 20 μL of stop solution, and their absorbance was measured at 405 nm.

Statistical Analysis

Statistical analysis was conducted using SPSS 21.0 (SPSS Inc., Chicago, IL, USA). The significance test depending on the treatment of GO coating did not meet the normality, thus the Mann–Whitney U -test, a non-parametric test, was performed. The significance of all data collected was tested at a significance level of $P < 0.05$.

Results

Surface Characteristics

Surface characteristics were observed with a scanning electron microscope (SEM) (Figure 2A and B). Group Zr exhibited an evenly polished surface, whereas in Group Zr-GO, GO exhibited a cloudy appearance on the surface.

Surface roughness was measured using a nanosurface 3D optical profiler (Figure 2C and D), with Group Zr-GO exhibiting high roughness ($n=3$). The R_a values of Group Zr and Zr-GO were 130.564 ± 50.352 nm and 184.084 ± 45.153 nm, respectively.

The atomic components of the surface were analyzed by XPS (Figure 3). Both Group Zr and Group Zr-GO exhibited oxygen (O), carbon (C), and zirconia (Zr) peaks. The element ratio analysis demonstrated that the Zr group consisted of 43.35% carbon, 45.28% oxygen, and 11.37% zirconia; and the Zr-GO group consisted of 86.78% carbon, 12.08% oxygen, and 1.13% zirconia. Group Zr-GO showed a high carbon peak, resulting in a 2x-high carbon ratio.

The Raman spectrum analysis (Figure 4) observed unique peaks of GO, including D band ($\sim 1350\text{cm}^{-1}$), G band ($\sim 1590\text{cm}^{-1}$), and 2D band ($\sim 2690\text{cm}^{-1}$). Compared with Group Zr, Group Zr-GO showed a significant increase in the contact angle ($39.27 \pm 0.914^\circ$ vs $64.64 \pm 0.310^\circ$; $P < 0.05$) (Figure 5).

Inhibition of Biofilm Formation

In the crystal violet assay, the *S. mutans* adhesion in Group Zr-GO significantly decreased compared to that of Group

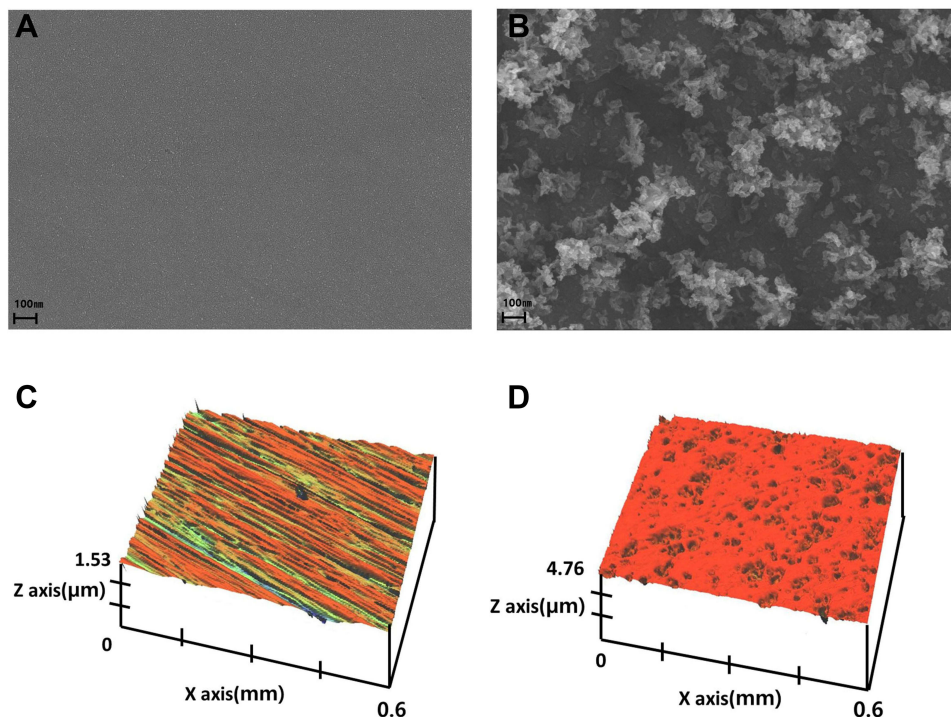


Figure 2 FE-SEM images of (A) control (Zr) and (B) GO-coated zirconia (Zr-GO) groups ($\times 50K$). Three-dimensional surface morphology roughness images of (C) Zr and (D) Zr-GO groups.

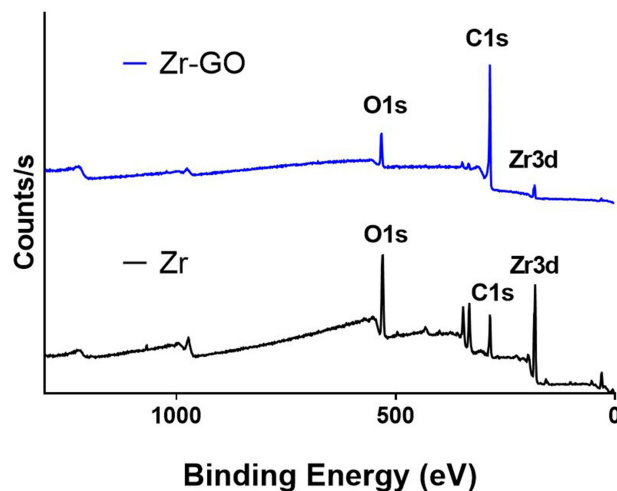


Figure 3 XPS profiles of GO-coated zirconia surface (Zr-GO) and control (Zr) groups.

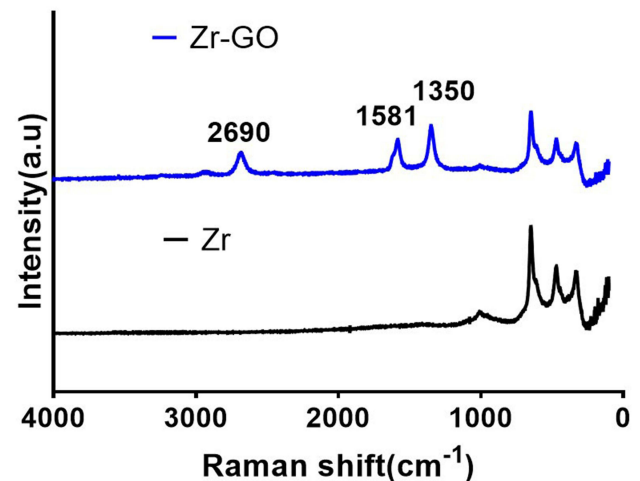


Figure 4 Raman spectrum of GO-coated zirconia surface (Zr-GO) and control (Zr) groups, showing D (1350 cm^{-1}), G (1581 cm^{-1}), and 2D peak at 2690 cm^{-1} of GO band.

Zr ($P < 0.001$) (Figure 6A). Additionally, the thickness of biofilm in Group Zr-GO decreased significantly (Group Zr = $16.99 \pm 3.36\ \mu\text{m}$, Group Zr-GO = $11.20 \pm 0.74\ \mu\text{m}$; $P < 0.05$) (Figure 6B). Finally, using the LIVE/DEAD[®] BacLight[™] Bacterial Viability Kit. (Figure 6C and D), a greater number of viable cells were observed in Zr group compared with that of the Zr-GO group.

Osteoblast Activation

Effects on Cell Adhesion, Proliferation, and Differentiation

To assess osteoblast adhesion and proliferation, the WST-8 assay was performed. For adhesion, a absorbance of Group Zr (2.18) was observed with a little higher than that of Group Zr-GO (0.207); however, this difference was not statistically

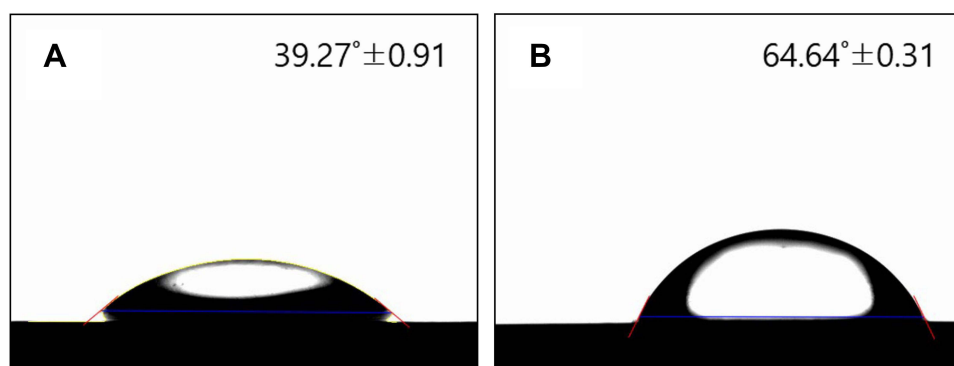


Figure 5 Water droplet on surface of the contact angle. **(A)** Control (Zr) group; **(B)** GO-coated zirconia (Zr-GO) group. The GO-coated zirconia (Zr-GO) group is hydrophobic compared to the control (Zr) group, and the contact angle was significantly increased.

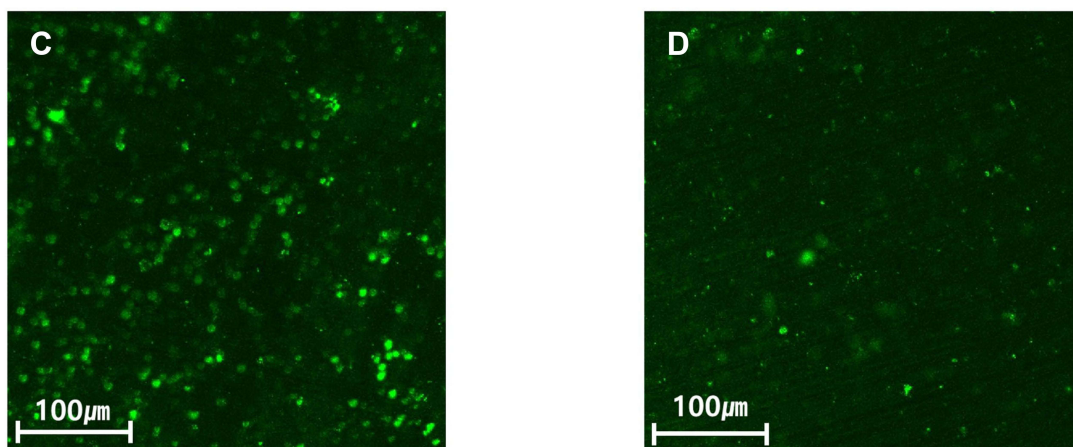
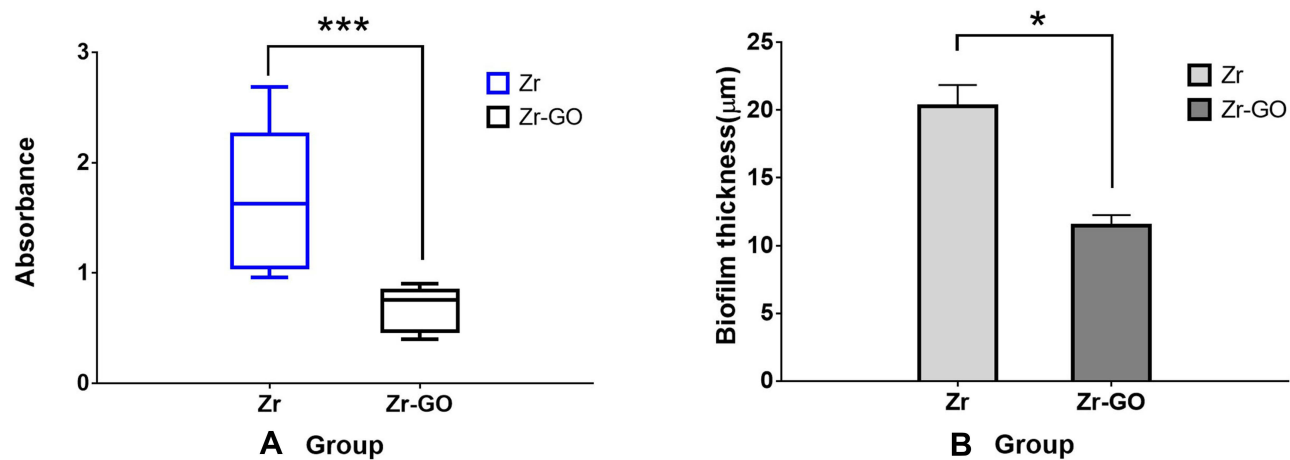


Figure 6 **(A)** Bacterial adhesion on GO-coated zirconia (Zr-GO) and control (Zr) surfaces, as measured by crystal violet assay ($n = 8$). **(B)** Biofilm thickness of *Streptococcus mutans* on Zr-GO and Zr surfaces ($n = 3$). **(C and D)** Viability of *Streptococcus mutans* biofilm on **(C)** Zr and **(D)** Zr-GO surfaces ($n = 3$). Green fluorescence indicates viable cells. * $P < 0.05$, *** $P < 0.001$; Mann–Whitney U -test.

significant (Figure 7A). Contrarily, for proliferation, a significantly higher absorbance level was observed in Group Zr-GO (0.322) as compared with that of Group Zr (0.309) ($P < 0.05$) (Figure 7B). Cell differentiation was

assessed using the ALP activity assay. As shown in Figure 7C, the absorbance level of Group Zr-GO (0.219) was significantly higher than that of Group Zr (0.190) ($P < 0.05$).

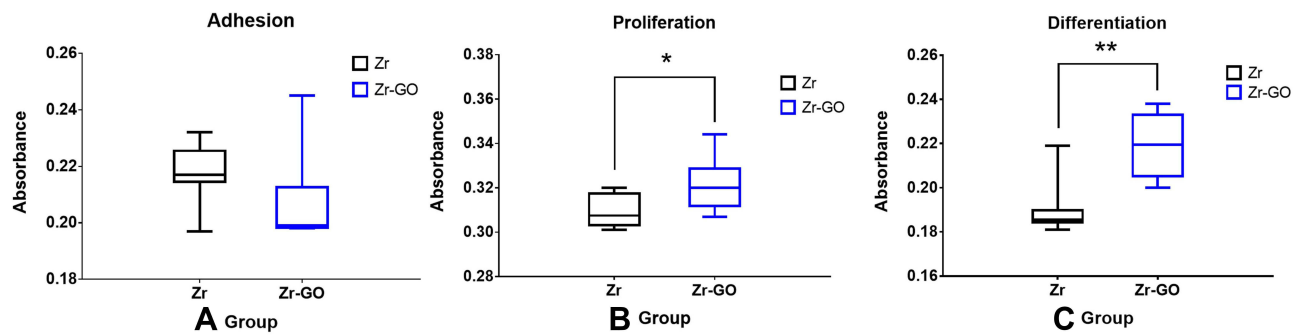


Figure 7 (A) Cell adhesion (measured using WST-8 assay at 24 h) on graphene oxide-coated zirconia (Zr-GO) and control (Zr) surfaces (n = 8). (B) Cell proliferation (measured using WST-8 assay at 120 h) on Zr and Zr-GO surfaces (n = 8). (C) Cell differentiation (measured by ALP assay at 21 days) on Zr and Zr-GO surfaces (n = 8). * $P < 0.05$, ** $P < 0.01$; Mann-Whitney *U*-test.

After the 5 days of cell culture, the proliferation of cell morphology were observed with a scanning electron microscope (SEM). It showed that the cells exhibited proliferation and spreading on the surfaces and the cells proliferated more in the group Zr-GO (Figure 8B–D). Than in the group Zr (Figure 8A–C) and a lot of cell projections were formed.

Discussion

Implants are very useful for replacing missing teeth. However, after implantation, bone resorption or inflammation of the surrounding gingiva often occurs because of bacterial infection. Therefore, to prevent this, researchers

have attempted to apply various surface treatments to the implant material to increase their success and survival rate; osseointegration and cell proliferation increased because of the increase of the surface roughness by treating the surface of the implant.³⁶ Electrochemical surface treatment³⁷ or application of an antibacterial material coatings have been also employed to reduce bacterial adhesion.⁸

Recently, several studies have exhibited an increased antibacterial activity of GO.^{40–42} A previous study by Liu and Qiu^{42,43} reported that treating surfaces with GO promoted antibiotic effects and bone activation. Additionally, Wang⁴⁴ reported that GO was effective in improving the bio-activation of the surface of materials. Fallatah et al⁴⁵

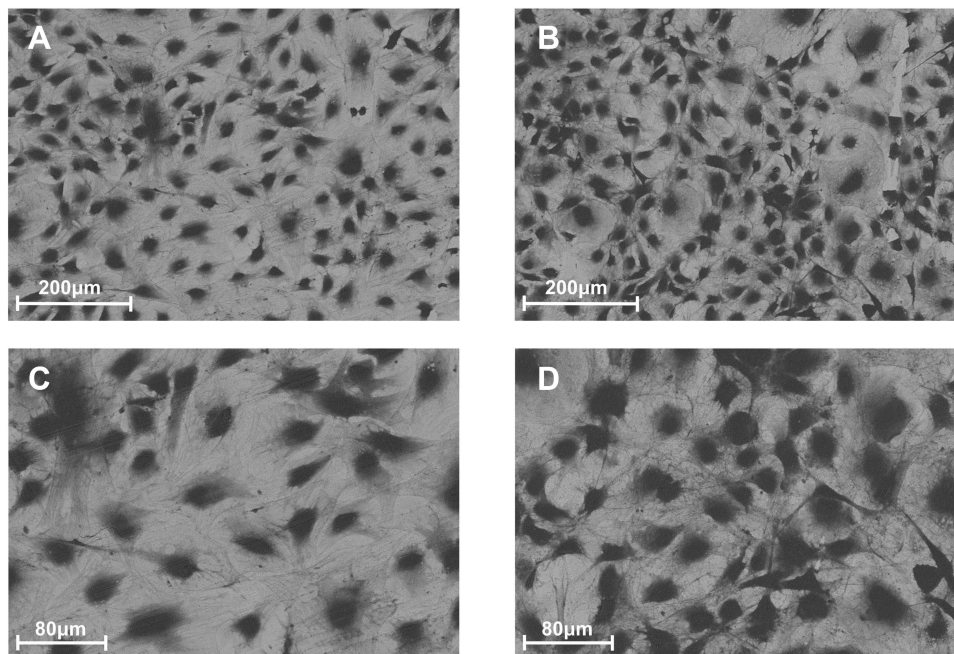


Figure 8 FE-SEM images of 5 days cell culture (A) Zr group: control group (x150K), (B) Zr-GO group: zirconia coated with GO (x150K), (C) Zr group: control group (x300K), (D) Zr-GO group: zirconia coated with GO (x300K).

demonstrated that GO reduced the biofilm thickness formed by *Pseudomonas putida* and had an ability to separate the biofilm from the surface. In this study, GO was directly deposited using argon plasma, which was cost-effective and did not generate any by-products on the zirconia surface. The bacteria resistance and cell activation levels were evaluated by treating GO on zirconia, which has a high corrosion resistance and biocompatibility similar to titanium and esthetics similar to the natural teeth.^{38,39}

The mechanism of antibacterial activity of GO remains to be elucidated. The antibacterial mechanism of GO known so far is the physical destruction of the cell membrane and oxidative stress damage.^{46,47} In general, it is known that reactive oxygen species (ROS)-mediated oxidative stress is generated by graphene-based materials, which causes serious damage to bacterial cells and has antibacterial action.^{48,49} However, some studies have conducted in vitro experiments and suggested that the ROS mechanism is not the primary mechanism for the antibacterial action of GO.^{38,50} Another antibacterial process is the dispersibility and trapping ability of oxygen-containing functional groups of GO.^{47,51–53} Due to the hydrophobic properties of graphene oxide, the adhesion of bacterial cells is prevented, and furthermore, the hydrophobic interaction can destroy the bacterial membrane, resulting in antibacterial action. Additionally, aggregated GO can serve as a scaffold for bacterial attachment and proliferation.⁵⁴ The antibacterial effect of GO and the effect of functional groups have received extensive attention for future studies.

In this study, *S. mutans* adhesion on GO-coated zirconia reduced significantly. This confirmed an antibacterial effect of GO, which aided in reducing the inflammation which might occur after the placement or restoration of zirconia implants. In addition to the antibacterial effect, the direct-deposited GO on zirconia also increased the cell activity which was effective in bone adhesion, proliferation, and differentiation. The hydrophobic and electrostatic interaction of GO improved bone differentiation resulting in its increased attention in the field of bone-tissue engineering.⁵⁵ Dinescu et al⁵⁶ evaluated bone differentiation by adding 3 wt% graphene to chitosan scaffolds and observed an increase in osteogenesis. This was attributed to the increased porosity of the surface which created a suitable environment for cell adhesion. Aidun et al⁵⁷ reported that (polycaprolactone) PCL-chitosan scaffolds that were additionally treated with GO showed an increase in the cell adhesion and proliferation, and the bioactivity and hydrophilicity of the surface, while maintaining their antibacterial effect. However, in this study, a significant difference was observed in osteoblast proliferation and differentiation whereas no significant change

was observed in cell adhesion. Unagolla et al⁵⁸ assessed cell adhesion of PCL scaffolds which were treated with graphene at different concentrations and reported significant increase in cell proliferation over time. However, cell adhesion did not show any significant difference between groups on the 2nd and 3rd day.

Hydrophilic surfaces exhibit increased adhesion and proliferation of bacteria and cells. In dentistry, various approaches have been applied to increase the surface hydrophilicity of implants. For example, Qu et al⁵⁹ reported that the surface of implants with high hydrophilicity can improve the adhesion and differentiation of surrounding cells. In this study, the contact angle of specimens in the untreated Group Zr and the GO-treated Group Zr-GO was compared. Group Zr demonstrated a relatively high hydrophilicity. This surface characteristic seemed to affect the early adhesion of cells, while coating zirconia with GO did not affect early adhesion and improved cell proliferation and differentiation.

Additionally, this study examined the effects of GO coating (on a zirconia surface) on the antibacterial activity and osteoblast activation. Earlier studies attempted to coat on titanium with ZrN or Ag nanos, which is known to have antibacterial effects, and applied it to the implant abutments.^{8,60–62} In addition, some studies suggested that bacteria living at the interface of implant abutment and prosthesis could be prevented.⁶³ Carinci et al⁶⁴ examined bacterial viability and biofilm formation on the inside of implants coated with chlorhexidine and reported that soft tissues were effectively healed without any inflammatory symptoms. These results demonstrated that zirconia coated with GO could be employed as a fixture and abutment while placing implants in the maxillary anterior area or in the interface of implants to reduce peri-implantitis. In addition, GO coating can be applied to the inner side of zirconia to produce dental crowns with a lower occurrence of secondary caries in abutments.

Conclusions

In this study, compared to the group Zr, the attachment of *S. mutans* was reduced by 58.58% and the biofilm thickness by 43.49% in the group Zr-GO. In cell evaluation, the adhesion of MC3T3-1 cells was not significant in group Zr and Zr-GO, but cell proliferation and cell differentiation increased by 3.23% and 15.79%, which were statistically significant.

This study confirmed the potential ability of zirconia implants coated with GO to inhibit biofilm formation and activate the cells. However, since GO has relatively low hydrophilicity compared with that of zirconia, additional research is required to increase the hydrophilicity of GO for a higher cell

activity. Moreover, when the layer of GO is too thick, the esthetic value of zirconia reduces. Therefore, it is important to determine the required minimum thickness of GO.

Acknowledgments

This work was supported by the National Research Foundation (NRF) of Korea grant funded by the Korea government (MSIP) (No. 2020R1F1A1076982 and 2018R1A2B6002268).

Disclosure

The authors report no conflicts of interest in this work.

References

- Han HJ, Kim S, Han DH. Multifactorial evaluation of implant failure: a 19-year retrospective study. *Int J Oral Maxillofac Implants.* 2014;29:303–310. doi:10.11607/jomi.2869
- Albouy JP, Abrahamsson I, Persson LG, Berglund T. Spontaneous progression of ligature induced peri-implantitis at implants with different surface characteristics. An experimental study in dogs II: histological observations. *Clin Oral Implants Res.* 2009;20:366–371. doi:10.1111/j.1600-0501.2008.01645.x
- Carcuac O, Abrahamsson I, Albouy JP, Linder E, Larsson L, Berglund T. Experimental periodontitis and peri-implantitis in dogs. *Clin Oral Implants Res.* 2013;24:363–371. doi:10.1111/clr.12067
- Lang NP, Bragger U, Walther D, Beamer B, Kornman KS. Ligature-induced peri-implant infection in cynomolgus monkeys. I. Clinical and radiographic findings. *Clin Oral Implants Res.* 1993;4:2–11. doi:10.1034/j.1600-0501.1993.040101.x
- Sanino G, Gigola P, Putini M, Pera F, Pasarielo C. Combination therapy including seratiopeptidase improves outcomes of mechanical-antibiotic treatment of perimplantitis. *Int J ImmunopatholPharmacol.* 2013;26(3):825–831. doi:10.1177/039463201302600332
- Park SY, Kim KH, Shin SY, et al. Decontamination methods using a dental water jet and dental flos for microthreaded implant fixtures in regenerative perimplantitis treatment. *Implant Dent.* 2015;24(3):307–316.
- Schwarz F, Bieling K, Bonsman M, Latz T, Becker J. Nonsurgical treatment of moderate and advanced perimplantitis lesions: a controlled clinical study. *Clin Oral Investig.* 2006;10(4):279–288.
- Wan R, Chu S, Wang X, et al. Study on the osteogenesis of rat mesenchymal stem cells and the long-term antibacterial activity of Staphylococcus epidermidis on the surface of silver-richTiN/Ag modified titanium alloy. *J Biomed Mater Res B Appl Biomater.* 2020;108(7):3008–3021.
- Chen H, Muller MB, Gilmore KJ, Wallace GG, Li D. Mechanically strong, electrically conductive, and biocompatible graphene paper. *Adv Mater.* 2008;20:3557–3561.
- Rao CNR, Sood AK, Subrahmanyam KS, Govindaraj A. Graphene: the new two dimensional nanomaterial. *Angew Chem Int Ed.* 2009;48:7752–7777. doi:10.1002/anie.200901678
- Fu C, Bai H, Zhu J, et al. Enhanced cell proliferation and osteogenic differentiation in electrospun PLGA/hydroxyapatite nanofiber scaffolds incorporated with graphene oxide. *PLoS One.* 2017;12:e0188352. doi:10.1371/journal.pone.0188352
- Su J, Du Z, Xiao L, et al. Graphene oxide coated titanium surfaces with osteoimmunomodulatory role to enhance osteogenesis. *Mater Sci Eng C Mater Bio Appl.* 2020;113:110983. doi:10.1016/j.msec.2020.110983
- Recinella L, Chiavari A, Giordani S, et al. Osteoblastic differentiation on graphene oxide-functionalized titanium surfaces: an in vitro study. *Nanomaterials.* 2020;10:654. doi:10.3390/nano10040654
- Nayak TR, Andersen H, Makam VS, et al. Graphene for controlled and accelerated osteogenic differentiation of human mesenchymal stem cells. *ACS Nano.* 2011;5:4670–4678. doi:10.1021/nn200500h
- Zhang L, Liu W, Yue C, et al. A tough graphene nanosheet/hydroxyapatite composite with improved in vitro biocompatibility. *Carbon.* 2013;61:105–115. doi:10.1016/j.carbon.2013.04.074
- Elkhenany H, Amelse L, Lafont A, et al. Graphene supports in vitro proliferation and osteogenic differentiation of goat adult mesenchymal stem cells: potential for bone tissue engineering. *J Appl Toxicol.* 2014;35:367–374. doi:10.1002/jat.3024
- Arshad A, Iqbal J, Siddiq M, et al. Graphene nanoplatelets induced tailoring in photocatalytic activity and antibacterial characteristics of MgO/graphene nanoplatelets nanocomposites. *J Appl Phys.* 2017;121:024901. doi:10.1063/1.4972970
- Novoselov KS. Electric field effect in atomically thin carbon films. *Science.* 2004;306(5696):666–669. doi:10.1126/science.1102896
- Rümmeli MH, Rocha CG, Ortman F, et al. Graphene: piecing it Together. *Adv Mater.* 2011;23:4471–4490. doi:10.1002/adma.201101855
- Brownson DAC, Banks CE. The electrochemistry of CVD graphene: progress and prospects. *Phys Chem Chem Phys.* 2012;14:8264. doi:10.1039/c2cp40225d
- Sali S, Mackey HR, Abdala AA. Effect of graphene oxide synthesis method on properties and performance of polysulfone-graphene oxide mixed matrix membranes. *Nanomaterials.* 2019;9:769. doi:10.3390/nano9050769
- Somanathan T, Prasad K, Ostrikov KK, Saravanan A, Krishna VM. Graphene oxide synthesis from agro waste. *Nanomaterials.* 2015;5:826–834. doi:10.3390/nano5020826
- Brownson DAC, Metters JP, Kampouris DK, Banks CE. Graphene electrochemistry: surfactants inherent to graphene can dramatically effect electrochemical processes. *Electroanalysis.* 2011;23:894–899. doi:10.1002/elan.201000708
- Brownson DAC, Banks CE. Graphene electrochemistry: surfactants inherent to graphene inhibit metal analysis. *Electrochem Commun.* 2011;13:111–113. doi:10.1016/j.elecom.2010.11.024
- Brownson DAC, Banks CE. Fabricating graphene supercapacitors: highlighting the impact of surfactants and moieties. *Chem Commun.* 2012;48:1425–1427. doi:10.1039/C1CC11276G
- Chu P, Chen JY, Wang LP, Huang N. Plasma-surface modification of biomaterials. *Mater Sci Eng R Rep.* 2002;36:143–206. doi:10.1016/S0927-796X(02)00004-9
- Park GY, Park SJ, Choi MY, et al. Atmospheric-pressure plasma sources for biomedical applications. *Plasma Sources Sci Technol.* 2012;21:043001. doi:10.1088/0963-0252/21/4/043001
- Bogya ES, Károly Z, Barabás R. Atmospheric plasma sprayed silica-hydroxyapatite coatings on magnesium alloy substrates. *Ceram Int.* 2015;41:6005–6012. doi:10.1016/j.ceramint.2015.01.041
- Wang L, Porto CL, Palumbo F, et al. Synthesis of antibacterial composite coating containing nanocapsules in an atmospheric pressure plasma. *Mater Sci Eng C Mater Biol Appl.* 2021;119:111496. doi:10.1016/j.msec.2020.111496
- Nicol MJ, Brubaker TR, Honish IIBJ, et al. Antibacterial effects of low temperature plasma generated by atmospheric-pressure plasma jet are mediated by reactive oxygen species. *Sci Rep.* 2020;10:3066. doi:10.1038/s41598-020-59652-6
- Rho KH, Park C, Alam K, et al. Biological effects of Plasma-based graphene oxide deposition on Titanium. *J Nanomater.* 2019;2019:1–7. doi:10.1155/2019/9124989
- Chevalier J. What Future for Zirconia as a Biomaterial? *Biomaterials.* 2006;27:535–543. doi:10.1016/j.biomaterials.2005.07.034
- Denry I, Kelly JR. State of the art of zirconia for dental applications. *Dent Mater.* 2008;24:299–307. doi:10.1016/j.dental.2007.05.007

34. Brüll F, Van Winkelhoff AJ, Cune MS. Zirconia dental implants: a clinical, radiographic, and microbiological evaluation up to 3 years. *Int J Oral Maxillofac Implants*. 2014;29:914–920. doi:10.11607/jomi.3293
35. Gautam C, Joyner J, Gautam A, Rao J, Vajtai R. Zirconia based dental ceramics: structure, mechanical properties, biocompatibility and applications. *Dalton Trans*. 2016;45:19194–19215. doi:10.1039/C6DT03484E
36. Jemat A, Ghazali MJ, Razali M, Otsuka Y. Surface modifications and their effects on titanium dental implants. *Biomed Res Int*. 2015;2015:1–11. doi:10.1155/2015/791725
37. Yu S, Guo D, Han J, et al. Enhancing antibacterial performance and biocompatibility of pure titanium by a two-step electrochemical surface coating. *ACS Appl Mater Interfaces*. 2020;12(40):44433–44446. doi:10.1021/acsami.0c10032
38. Zhao M, Shan T, Wu Q, Gu L. The Antibacterial effect of graphene oxide on streptococcus mutans. *J Nanosci Nanotechnol*. 2020;20:2095–2103. doi:10.1166/jnn.2020.17319
39. Vi TTT, Kumar SR, Pang JHS, Liu YK, Chen DW, Lue SJ. Synergistic antibacterial activity of silver-loaded graphene oxide towards staphylococcus aureus and escherichia coli. *Nanomaterials(Basel)*. 2020;10:366. doi:10.3390/nano10020366
40. Hu WB, Peng C, Luo WJ, et al. Graphene based antibacterial paper. *ACS Nano*. 2010;4:4317–4323. doi:10.1021/nn101097v
41. Zou XF, Zhang L, Wang ZJ, Luo Y. Mechanisms of the antimicrobial activities of graphene materials. *J Am Chem Soc*. 2016;138:2064–2077. doi:10.1021/jacs.5b11411
42. Qiu J, Geng H, Wang D, et al. Layer-number dependent antibacterial and osteogenic behaviors of graphene oxide electrophoretic deposited on titanium. *ACS Appl Mater Interfaces*. 2017;9:12253–12263. doi:10.1021/acsami.7b00314
43. Liu M, Hao L, Huang Q, et al. Tea polyphenol-reduced graphene oxide deposition on titanium surface enhances osteoblast bioactivity. *J Nanosci Nanotechnol*. 2018;18(5):3134–3140. doi:10.1166/jnn.2018.14649
44. Wang C, Hu H, Li Z, et al. Enhanced osseointegration of titanium alloy implants with laser micro grooved surfaces and graphene oxide coating. *ACS Appl Mater Interfaces*. 2019;11:39470–39483. doi:10.1021/acsami.9b12733
45. Fallatah H, Elhaneid M, Ali-Boucetta H, Overton TW, El Kadri H, Gkatzionis K. Antibacterial effect of graphene oxide (GO) nano-particles against *Pseudomonas putida* biofilm of variable age. *Environ Sci Pollut Res Int*. 2019;26:25057–25070. doi:10.1007/s11356-019-05688-9
46. Li X, Li F, Gao Z, Fang L. Toxicology of graphene oxide nanosheets against *paecilomyces catenulatus*. *Bull Environ Contam Toxicol*. 2015;95(1):25–30. doi:10.1007/s00128-015-1499-3
47. Zou X, Zhang L, Wang Z, Luo Y. Mechanisms of the antimicrobial activities of graphene materials. *J Am Chem Soc*. 2016;138(7):2064–2077.
48. Zhang Y, Ali SF, Dervishi E, et al. Cytotoxicity effects of graphene and single-wall carbon nanotubes in neural pheochromocytoma-derived PC12 cells. *ACS Nano*. 2010;4(6):3181–3186. doi:10.1021/nn1007176
49. Gurunathan S, Han JW, Dayem AA, et al. Antibacterial activity of dithiothreitol reduced graphene oxide. *J Industrial Eng Chem*. 2013;19(4):1280–1288. doi:10.1016/j.jiec.2012.12.029
50. Kurantowicz N, Sawosz E, Jaworski S, et al. Interaction of graphene family materials with *Listeria monocytogenes* and *Salmonella enterica*. *Nanoscale Res Lett*. 2015;10:23–34. doi:10.1186/s11671-015-0749-y
51. Liu S, Zeng TH, Hofmann M, et al. Antibacterial activity of graphite, graphite oxide, graphene oxide, and reduced graphene oxide: membrane and oxidative stress. *ACS Nano*. 2011;5(9):6971–6980. doi:10.1021/nn202451x
52. Akhavan O, Ghaderi E, Esfandiari A. Wrapping bacteria by graphene nanosheets for isolation from environment, reactivation by sonication, and inactivation by near-infrared irradiation. *J Phys Chem B*. 2011;115(19):6279–6288. doi:10.1021/jp200686k
53. Akhavan O, Ghaderi E. Escherichia coli bacteria reduce graphene oxide to bactericidal graphene in a self-limiting manner. *Carbon*. 2012;50(5):1853–1860. doi:10.1016/j.carbon.2011.12.035
54. Ruiz ON, Fernando KA, Wang B, et al. Graphene oxide: a nonspecific enhancer of cellular growth. *ACS Nano*. 2011;5(10):8100–8107. doi:10.1021/nn202699t
55. Hermenean A, Codreanu A, Herman H, et al. Chitosan-graphene oxide 3D scaffolds as promising tools for bone regeneration in critical-size mouse calvarial defects. *Sci Rep*. 2017;7:91–95. doi:10.1038/s41598-017-16599-5
56. Dinescu S, Ionita M, Ignat SR, Costache M, Hermenean A. Graphene oxide enhances chitosan-based 3d scaffold properties for bone tissue engineering. *Int J Mol Sci*. 2019;20:5077. doi:10.3390/ijms20205077
57. Aidun A, Safaei Firoozabady A, Moharrami M, et al. Graphene oxide incorporated polycaprolactone/chitosan/collagen electrospun scaffold: enhanced osteogenic properties for bone tissue engineering. *Artif Organs*. 2019;43(10):E264–E281. doi:10.1111/aor.13474
58. Unagolla JM, Jayasuriya AC. Enhanced cell functions on graphene oxide incorporated 3D printed polycaprolactone scaffolds. *Mater Sci Eng*. 2019;102:1–11. doi:10.1016/j.msec.2019.04.026
59. Qu Z, Rausch-Fan X, Wieland M, Matejka M, Schedle A. The initial attachment and subsequent behavior regulation of osteoblasts by dental implant surface modification. *J Biomed Mater Res A*. 2007;82:658–668.
60. Brunello G, Brun P, Gardin C, et al. Biocompatibility and antibacterial properties of zirconium nitride coating on titanium abutments: an in vitro study. *PLoS One*. 2018;13:e0199591.
61. Kheur S, Singh N, Bodas D, et al. Nanoscale silver depositions inhibit microbial colonization and improve biocompatibility of titanium abutments. *Colloids Surf B Biointerfaces*. 2017;159:151–158.
62. Slate AJ, Wickens DJ. Antimicrobial activity of Ti-ZrN/Ag coatings for use in biomaterial applications. *Sci Rep*. 2018;8:1497.
63. Scarano A, Valbonetti L, Degidi M, Pecci R, Piattelli A. Implant-abutment contact surfaces and microgap measurements of different implant connections under 3-dimensional X-ray microtomography. *Implant Dent*. 2016;25:656–662.
64. Carinci F, Lauritano D, Bignozzi CA, et al. A new strategy against peri-implantitis: antibacterial internal coating. *Int J Mol Sci*. 2019;20:3897.

International Journal of Nanomedicine

Publish your work in this journal

The International Journal of Nanomedicine is an international, peer-reviewed journal focusing on the application of nanotechnology in diagnostics, therapeutics, and drug delivery systems throughout the biomedical field. This journal is indexed on PubMed Central, MedLine, CAS, SciSearch®, Current Contents®/Clinical Medicine,

Submit your manuscript here: <https://www.dovepress.com/international-journal-of-nanomedicine-journal>

Dovepress

Journal Citation Reports/Science Edition, EMBASE, Scopus and the Elsevier Bibliographic databases. The manuscript management system is completely online and includes a very quick and fair peer-review system, which is all easy to use. Visit <http://www.dovepress.com/testimonials.php> to read real quotes from published authors.